Detection of thin cirrus using a combination of 1.38-μm reflectance and window brightness temperature difference

J. K. Roskovensky and K. N. Liou

Department of Atmospheric Sciences, University of California, Los Angeles, California, USA

Received 20 December 2002; revised 28 April 2003; accepted 20 May 2003; published 17 September 2003.

[1] A new cloud-detection scheme has been developed that utilizes 1.38-μm reflectance in combination with 8.6–11 μm brightness temperature difference ($BTD_{8.6-11}$) to detect thin cirrus clouds. The 1.38-μm channel of the moderate resolution imaging spectroradiometer (MODIS) is useful in detecting thin cirrus due to its high sensitivity to upper tropospheric clouds and a nearly negligible sensitivity to low-level reflectance. Dependent upon neighboring cloud type, water vapor concentration, and the viewing geometry, specific 1.38-μm reflectance threshold levels can be utilized to detect thin cirrus that has previously been undetectable by downward looking satellite imagery. $BTD_{8.6-11}$ is also sensitive to ice clouds and is used as a second, independent, cirrus cloud test. Each test can either support or negate results from the other. Final cloud type results are produced by using cirrus detected by either the 1.38-μm reflectance test or the $BTD_{8.6-11}$ test or by using only that detected by both tests depending on whether a sizable amount of the neighboring cloud is opaque or not as determined by a simple visible reflectance test. It is found that 1.38-μm reflectance can often detect a greater amount of thin cirrus than the $BTD_{8.6-11}$. Satellite data from 10 MODIS cases over the atmospheric radiation measurement-tropical western Pacific and southern Great Plains sites were chosen because they provide land and ocean surface cases, variation in cloud type to test the algorithms reliability, and ground truth in the form of millimeter-wave radar data. Two-dimensional horizontal cloud type detection results are shown to correlate well with the 1-hour cloud radar reflectivity time series centered at the MODIS overpass time. Statistics indicate that the new algorithm more accurately identifies thin cirrus in cases involving only single-layer cirrus and where thin cirrus overrides low cloud. *INDEX TERMS:* 3360 Meteorology and Atmospheric Dynamics: Remote sensing; 3359 Meteorology and Atmospheric Dynamics: Radiative processes; 3394 Meteorology and Atmospheric Dynamics: Instruments and techniques; *KEYWORDS:* cirrus, MODIS, clouds

Citation: Roskovensky, J. K., and K. N. Liou, Detection of thin cirrus using a combination of 1.38-μm reflectance and window brightness temperature difference, *J. Geophys. Res.*, *108*(D18), 4570, doi:10.1029/2002JD003346, 2003.

1. Introduction

[2] The presence of optically thin cirrus clouds is an important factor in the variation of the global radiation budget and terrestrial thermal balance. It is possible to retrieve thin cirrus cloud properties from satellite data using existing algorithms [e.g., *Ou et al.*, 1999; *Rolland et al.*, 2000; *Rolland and Liou*, 2001], provided these thin cirrus clouds can be properly identified. However, the detection of visual and subvisual thin cirrus clouds is a subject still under development. As a consequence, limited cirrus cloud climatologies established in the past may have been underestimating the thin cirrus cloud cover. Using a low-resolution CO_2 slicing method, *Wylie et al.* [1994] estimated that thin cirrus ($\tau < 0.7$) covers about 20% of the midlatitude region and over 50% of the tropics. Limited global cirrus maps based on the moderate resolution imaging spectroradiometer (MODIS) cloud mask algorithm (S. A. Ackerman et al., Discriminating clear-sky from cloud with MODIS algorithm theoretical basis document (MOD35), ATBD-MOD-06, version 6.0, 115 pp., 2002, available at http://modis.gsfc.nasa.gov/data/atbd/atmos_atbd.html), which includes data from the 1.38-μm channel, show that the global cirrus cloud coverage is less than that demonstrated by Wylie et al. using the high-resolution infrared radiation sounder (HIRS) channels. Nevertheless, cirrus clouds occur at all latitudes and their global fractional coverage remains in question.

[3] To investigate the possibility of detecting thin cirrus clouds using high-resolution images from spectroradiometer channels, *Gao et al.* [1993] showed that the reflectance of the airborne visible/infrared imaging spectrometer (AVIRIS) 1.38-μm channel, located in a strong water vapor absorption band, is particularly sensitive to the presence of high-level cirrus clouds. When a significant amount of water vapor is present in the atmosphere, the radiation at this wavelength is completely absorbed within the lower levels. Therefore only

0148-0227/03/2002JD003346$09.00

reflection off midlevel and high-level clouds is able to reach the satellite sensor, and strong reflectance in this channel can be entirely attributed to upper tropospheric clouds. It is noted that the reflectance of the MODIS airborne simulator (MAS) 1.90-μm channel, a water vapor absorption channel, and a surrogate for the1.38-μm channel, is also sensitive to the presence of thin cirrus clouds [*King et al.*, 1996] in the same manner. *Hutchinson and Choe* [1996] showed that the use of 1.38-μm reflectance thresholds using AVIRIS data significantly improved the accuracy of identifying thin cirrus clouds over methods based on advanced very high resolution radiometer (AVHRR) data for all types of ground surfaces. They also determined that the AVIRIS 1.38-μm narrow band channel did not mask all of the incident energy passing through low levels. As a result, they concluded that surface albedo and water vapor concentrations should be taken into account when determining appropriate 1.38-μm reflectance thresholds.

[4] The purpose of this study is to investigate the possibility of improving thin cirrus detection by using the MODIS 1.38-μm reflectance data on board the Terra satellite. In order to do this, we have developed a new cloud-detection scheme that employs 1.38-μm reflectances as the primary tool in detecting high ice clouds and the window brightness temperature difference between 8.6 and 11 μm ($BTD_{8.6-11}$) as a second, independent test to either reinforce or negate the 1.38-μm reflection results. We compare this scheme with two other cloud type detection algorithms: a simple scheme based on three variables from the MODIS cloud mask product (MOD35) that we have developed and a routine based on the cloud phase identification algorithm of *Ou et al.* [1996]. All of these algorithms are able to separate pixels into at least four different regimes: clear, low-cloud, single-layer cirrus, and multilayer cloud which is either cirrus above low cloud or opaque high cloud. Further comparison is made with the MODIS level-2 cloud phase product (MOD06). Validation will be obtained by matching these cloud type results in space to both ground-based millimeter-wave radar measurements in time. At this time, we examine only tropical ocean and midlatitude continental regions due to the availability of ground instruments used for validation. Results indicate that this new algorithm is useful in detecting thin cirrus and may complement existing operational cloud-detection schemes in the specific regions previously noted. Further case studies over dry and cold regions such as subtropical deserts, polar and high-altitude areas need to be examined before this scheme can be utilized globally.

[5] This paper is organized as follows. In section 2, we describe the data sources that are used in this study. Section 3 describes the new cloud-detection algorithm in more detail and includes the rationale behind using each cirrus test and an explanation about how all of the required threshold values are determined. Results of several case studies are presented in depth in section 4, where each case is separated into scenes with either ocean or land surfaces. Finally, a summation is given in section 5.

2. Data Sources

[6] The atmospheric radiation measurement (ARM) program has established several cloud and radiation test beds (CART), which consist of a high concentration of atmospheric measuring instruments. Data from two of these sites, Lamont, Oklahoma in the southern Great Plains (SGP) site and the Republic of Nauru in the tropical western Pacific (TWP) site, were used in determining atmospheric conditions during the period surrounding specific MODIS overpasses. Cloud heights and thicknesses were found using continuous millimeter-wave radar reflectivity data. Wind speed and direction were available from the balloon-borne sounding system and continuous radar wind profiler data. Column water vapor amounts were obtained from microwave radiometers. Data from the 1-hour period centered on a MODIS overpass were most important.

[7] The MODIS instrument consists of 36 narrow band channels from 0.41 to 14.2 μm. The following four channels were used in our cloud type identification algorithm: 0.65 μm (band 1), 1.38 μm (band 26), 8.60 μm (band 29), and 11.03 μm (band 31). Two additional channels, 0.86 μm (band 2) and 12.02 μm (band 32), were used to simulate results from the cloud type detection algorithm of *Ou et al.* [1996]. Reflection and radiance data were taken from the 1 × 1 km (nadir) aggregate data set of the level 1-B data product (MOD02). Radiance from bands 29, 31, and 32 were converted into brightness temperatures that were compared with the brightness temperature at 5 × 5 km resolution from the cloud properties product (MOD06) for accuracy. All calculated brightness temperatures were well within 0.1 K of the MOD06 results. Additional clear-sky and cloud information was available from the cloud mask product (MOD35) at 1 × 1 km nadir resolution. We have reprocessed the MODIS 1.38-μm data from the MOD02 granules to remove known contamination from the 1.24-μm band using correction coefficients determined by C. Moeller (private communication, 2002) of the University of Wisconsin. As a result, mean clear-sky 1.38-μm reflectance from the SGP sites decreased from 1.3 to 0.9% while mean low-cloud reflectance dropped from 1.8 to 0.9%. This procedure appears to have removed most of the low-level 1.24-μm signal impinging upon the 1.38-μm data and suggests that any further contamination from nonabsorbing channels is minor since the average clear-sky and low-cloud 1.38-μm reflectances became equal after the correction as would be expected.

[8] In order to limit the scale of our examination, only data over the rectangular regions of the ARM-CART sites were considered. The SGP region was defined between the latitudes of 34.5°N and 39°N and in longitude between 100°W and 95°W at approximately 1-km resolution. This resulted in a grid with 456 pixels in the east-west direction and 501 pixels in the north-south direction. A section of the TWP site centered over Nauru was defined between 0.5°N, 2.5°S, 165°E, and 169°E. This provided a 1-km resolution grid of 333 by 444 pixels in the north-south and east-west directions, respectively. To fit MODIS data, whose scan lines are orientated at an angle with respect to the vertical and horizontal grid lines of the defined ARM regions and whose resolution is generally greater than its 1 × 1 km nadir field of view, a grid point fitting and filling routine was developed. This was carried out by first finding the latitude and longitude for each MODIS pixel through bilinear interpolation, because the MODIS location is determined at only 5 × 5 km resolution (every fifth pixel). Each

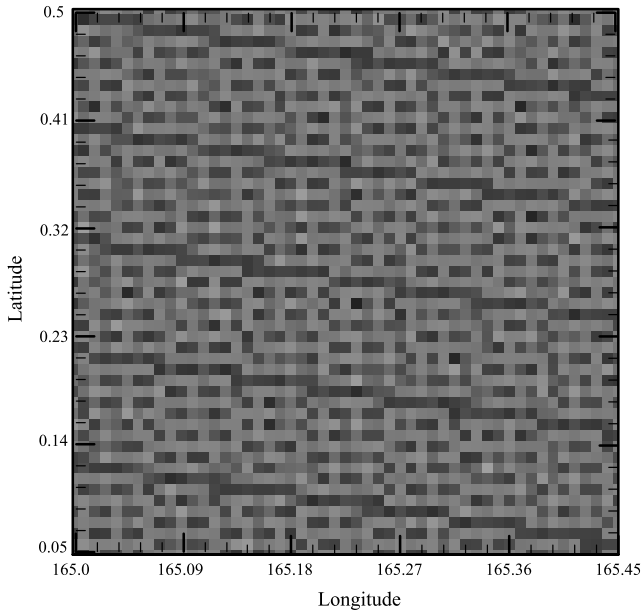

Figure 1. The MODIS data filling routine after one pass through a granule. Dark spaces indicate grid points that were filled, while lighter gray shows the nonfilled points. Roughly, one half of the grid points are initially filled after this pass. The plot represents the 50 × 50 km region in the northwest section of a defined TWP-ARM region for the 17 August 2001 case. Latitude is given in degrees north, while longitude is in degrees east.

MODIS pixel inside the defined ARM region is then fitted to the closest ARM grid point and MODIS data are stored at that location. This procedure generally fills roughly one half of the ARM grid points, shown in Figure 1 as dark spaces in a 50 × 50 km region of a TWP scene. To fill the remaining spaces with data, an averaging scheme is used whereby each empty grid point is filled by the mean value of the data from all adjacent grid points that contain data (maximum eight points). This scheme is successively run until every ARM grid point is filled with data.

[9] Ten MODIS granules were selected that offer variation in cloud type over both land and water surfaces, in addition to their proximity to ground instruments of the ARM-CART sites. Time series from the vertically pointing cloud radars on the Republic of Nauru (TWP) and at the central facilities near Lamont, Oklahoma (SGP), provided the vertical cloud structures during the MODIS overpasses that were used to determine the cloud type and to select the scenes. It was necessary to examine a variety of cloud scenes to test our cloud type detection algorithm. In particular, both clear-sky and low-cloud cases were important to determine the accuracy of the cloud scheme. The following seven cloud scenes, all from 2001 and listed in chronological order, were selected over the SGP site where the MODIS overpass time, in UT, is stated in parentheses: (1) 11 February (1731), continuous thin cirrus, (2) 6 March (1736), continuous thick cirrus, (3) 22 March (1735), continuous thin cirrus, (4) 29 March (1742), stratus, (5) 14 April (1741), scattered cirrus over stratus, (6) 16 April (1729), altostratus, and (7) 25 May (1734), clear sky and cumulus. The three scenes chosen over the TWP site (also from 2001) are: (1) 16 August (2310), continuous thin cirrus over scattered cumulus, (2) 17 August (2353), cumulus giving way to clear sky, and (3) 25 August (2304), cumulus.

3. A New Thin Cirrus Cloud-Detection Scheme

[10] The 1.38-μm channel on MODIS has the potential to greatly improve high-cloud detection capabilities. Our objective is to obtain a correct reflectance threshold in order to detect high thin clouds, but at the same time, exclude false detection from clear and low-cloud pixels. Establishing reasonable bounds for this threshold is necessary. A good minimum bound is the actual clear-sky 1.38-μm reflectance as determined separately for each MODIS granule. In order to identify an appropriate upper bound, theoretical clear sky and thin cirrus 1.38-μm reflectance was calculated over a broad range of satellite viewing angles (−50° to 50°) and solar angles (0°–60°). The radiative transfer code used to make the calculations is based upon the adding/doubling method [*Takano and Liou*, 1989b] which takes atmospheric gaseous absorption including that of water vapor into account and incorporates scattering from nonspherical, randomly orientated ice crystals defined by the cold cirrus size distribution of *Heymsfield and Platt* [1984] and *Takano and Liou* [1989a] with effective particle size of 24 μm. Figure 2 shows the clear-sky and thin cirrus reflection results for a constant solar zenith angle of 32° and relative azimuthal angles of 5° (positive satellite

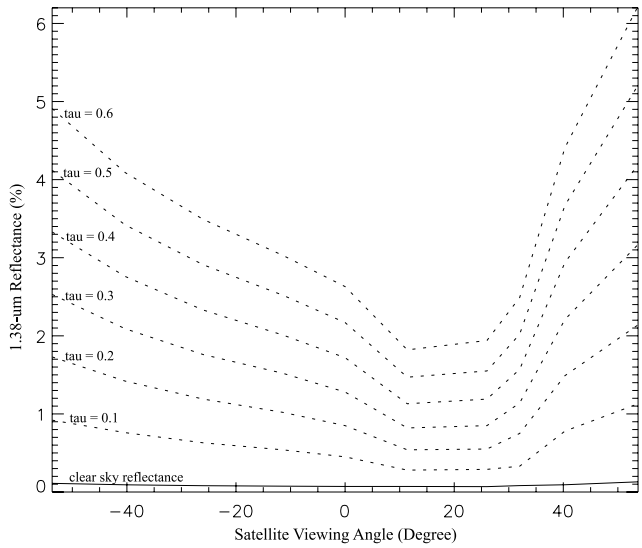

Figure 2. Theoretical 1.38-μm reflectance for clear sky (solid curve) and cirrus clouds (dashed curves) with optical depths (τ) between 0.1 and 0.6. The solar zenith angle was 32°, while a relative azimuthal angle of 5° was used for positive satellite viewing angles and 175° was used for negative angles. Calculations were made using 0.5% surface reflectance, continental aerosol size distribution with optical depth of 0.32, and a cirrus cloud 2.3-km thick with cloud top of 10 km using the cold cirrus size distribution from the work of *Heymsfield and Platt* [1984] and *Takano and Liou* [1989a] with effective particle size of 24 μm.

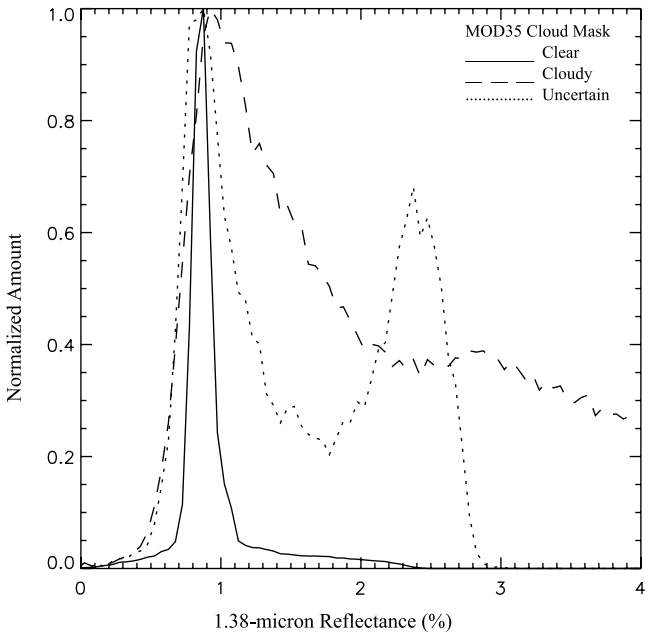

Figure 3. Normalized 1.38-μm reflectance for three MODIS cloud mask CSP groups is presented for the 15 October 2000 scene over the SGP-ARM site. The solid curve represents clear pixels with CSP greater than 95%. The dashed curve represents cloudy pixels with CSP less than 66%. The dotted curve shows the uncertain pixels with CSP between 66 and 95%. There appears to be a distinct separation of the uncertain pixels between those with a high-cloud component (second peak in 1.38-μm reflection above 1.8%) and those without. Total pixels examined in the clear, uncertain, and cloudy groups were 62,009, 1348, and 8723, respectively.

scan angles) and 175° (negative satellite scan angles). It can be seen that 1.38-μm reflectance is not isotropic and varies significantly with cloud optical depth and scan angle. Based upon the region of minimum reflectance (10°–30° scan angle) it can be seen that all cirrus clouds with optical depth greater than about 0.8 (from extrapolation of the curves in Figure 2) should be detectable with a 2.5% 1.38-μm reflectance level. Although somewhat arbitrary, this level provides a good upper bound for the two ARM site regions because it is located well above expected clear-sky reflectance but not so high as to be unable to detect thick cirrus clouds. The use of five 1.38-μm reflectance thresholds between 2.5% and the theoretical clear-sky reflectance provides an effective range of values with distinct intervals on the order of 0.4% in which to identify the best threshold for thin cirrus detection. The ideal threshold will ultimately be found in each scene by comparison with the cloud radar results.

[11] Consequently, five 1.38-μm reflectance thresholds were defined as a function of satellite scan angle at intervals of 1° for each scene, using the difference between the mean observed clear-sky reflectance and 2.5% (d = 2.5 − mean clear-sky reflectance). This difference was then divided by six (d/6) in order to produce five separate threshold levels by adding this new small difference to the mean clear-sky reflectance n number of times. For example, the lowest threshold, T1, was determined as the mean clear-sky reflectance + d/6 and the next, T2, by the mean clear-sky reflectance + 2(d/6), and so forth. Cirrus 1.38-μm reflectance, which is proportional to the solar angle, could vary considerably during the year. In this regard, the best of the five cirrus thresholds may have a seasonal dependence especially at the SGP-ARM site due to the larger range in expected solar angles (roughly 15°–63°). Although not examined in this paper, lower thresholds would appear to be necessary during times with small solar zenith angles such as summer at the SGP site and March and September at the TWP site.

[12] Figure 3 highlights both the potential advantages and concerns of examining 1.38-μm reflection data to identify thin cirrus. The normalized histogram of three clear-sky probability (CSP) groups for a MODIS granule on 15 October 2000 at 1725 UT shows that some pixels deemed as high-probability clear (>95%) by the CSP variable from the MODIS cloud mask product have a higher reflectance than pixels classified as cloudy (<66%). This could indicate that very thin cirrus went undetected. In addition, cirrus clouds are likely to be present in the second peak in reflectance, near 2.5%, of the uncertain pixels defined by CSP values between 66 and 95%. The cloudy pixels prove to be more difficult to interpret even though the initial peak is at the same location as the clear-sky peak (0.9%) and is probably due to low cloud. Yet because there is a more continuous distribution from low to high reflection, separating the high cloud from this group may require additional information.

[13] The $BTD_{8.6-11}$ threshold test is employed to aid in separating ice cloud from water cloud. Clear-sky transmittance of 8.6-μm radiation is lower than that of 11 μm due to greater water vapor absorption at the smaller wavelength. Thus clear-sky $BTD_{8.6-11}$ is expected to be negative. Since ice particles absorb much less radiation at 8.6 μm than at 11 μm, cirrus clouds produce large positive $BTD_{8.6-11}$ (>1) values. For liquid water, the imaginary index of refraction increases roughly 2.6 times less between 8.6 and 11 μm [*Downing and Williams*, 1975] than it does for ice [*Warren*, 1984] so that low clouds are not expected to register as high $BTD_{8.6-11}$ values as cirrus clouds. By establishing both scene clear and low-cloud thresholds (one standard deviation greater than the mean values without any geometry dependence, discussed below), we find that cirrus pixels can be identified as those having $BTD_{8.6-11}$ values exceeding these thresholds. Figure 4 shows theoretical $BTD_{8.6-11}$ as a function of cloud optical depth for a cirrus cloud located between 8 and 10 km in height with effective particle size of 24 μm, and separately, for a water cloud with effective particle radius of 12 μm at an altitude of 3–4 km. For clouds with optical depth (τ) greater than 0.5, there is a clear difference in $BTD_{8.6-11}$ between ice and water cloud. The smaller difference between ice and water cloud $BTD_{8.6-11}$ with optical depths less than 0.5 may make it difficult to decipher very thin cirrus from thin water clouds with this test. While both of the cirrus tests seem to be able to detect thin cirrus, $BTD_{8.6-11}$ values from thin cirrus can be overshadowed by those of thin water clouds, and thin cirrus 1.38-μm reflectance may be similar to that of thick water clouds if the above cloud water vapor path is small. Using the two tests simultaneously can insure that both thick and

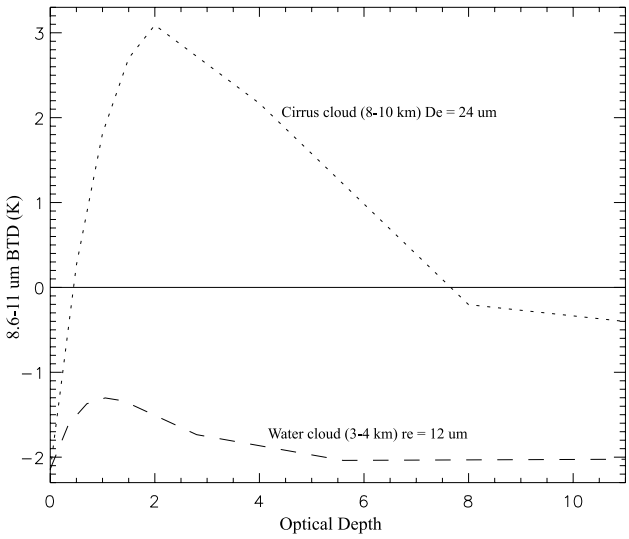

Figure 4. Theoretical 8.6−11 μm BTD measured in kelvins plotted against cloud optical depth for an ice cloud (dotted curve) and water cloud (dashed curve). The simulated ice cloud is 2-km thick with cloud top at 10 km and particle size distribution as described by *Heymsfield and Platt* [1984] and *Takano and Liou* [1989b] with effective size parameter of 24 μm, while the water cloud is 1-km thick and located between 3 and 4 km with effective particle radius of 12 μm.

thin water clouds are prevented from being falsely detected as high cloud.

[14] Clear-sky, thin cirrus, and low-cloud thresholds are calculated for each scene before the cloud detection algorithm is run. Clear-sky pixels are identified if CSP is greater than 95%, 1.38-μm reflectance is less than 1.1%, and the $BTD_{8.6-11}$ is less than −0.5 K. These values were chosen to eliminate clouds, especially thin cirrus based on theoretical computations and clear-sky MODIS observations. Thin cirrus pixels are then identified as those pixels that are not clear and possess 1.38-μm reflectance greater than 2% and 0.65-μm reflectance less than 20%, while low-cloud pixels require 1.38-μm reflectance less than 2% and 0.65-μm reflectance greater than 20%. These values insure that only thin cirrus pixels are used when the 0.65-μm reflectance is less than 20%, and only low-cloud pixels are found when 1.38-μm reflectance is less than 2%. Figure 5a shows the five 1.38-μm reflectance thresholds and Figure 5b shows the 0.65-μm reflectance thresholds for the 22 March case. The T1 1.38-μm reflectance threshold shows the greatest variance with scan angle since it is most affected by the mean clear-sky reflectance. The subsequent thresholds, T2–T5, become smoother as their distance to the constant 2.5% upper bound becomes smaller. Both 0.65-μm clear and cirrus cloud thresholds are found by adding one standard deviation to the mean reflectance as a function of satellite scan angle. These curves can be smoothed to remove excessive variance produced by insufficient data such as seen near the scan angle of 33° in Figure 5b. Table 1 shows the average 1.38-μm reflectance, 0.65-μm reflectance, and $BTD_{8.6-11}$ thresholds for the combined SGP and TWP cases. The only major differences between the SGP and the TWP values are the smaller 0.65-μm reflectance thresholds due to the lower surface reflection of the ocean to that of the land. The higher $BTD_{8.6-11}$ thresholds of the TWP site cannot be attributed to anything physical because of the small data set. It is also noted that mean $BTD_{8.6-11}$ values varied by as much as 1 K between scenes.

[15] Figure 6 shows the flowchart describing the steps of the new cloud type detection scheme developed to incorporate the new 1.38-μm reflectance and $BTD_{8.6-11}$ thresholds. Every pixel is examined in two separate passes. There are 10 cloud products generated by the first pass (Figure 6a) since two versions are created for each of the five 1.38-μm reflectance thresholds. The first version requires that both the 1.38-μm reflectance test and the $BTD_{8.6-11}$ test must detect cirrus at that pixel. This will be referred to as the AND result. The second version, the OR result, allows cirrus detection to be made by only one of the two cirrus tests. Initially, pixels with poor data quality and those water surface pixels flagged as affected by sun glint by the MODIS cloud mask product, are eliminated. Second, clear-sky pixels are identified if the CSP is greater than 95%, the 1.38-μm reflectance is less than the threshold being used, and the $BTD_{8.6-11}$ value is less than the clear-sky threshold ($BTD_{8.6-11\ TClr}$). Next, opaque ice clouds are separated if a pixel has an 11-μm brightness temperature (BT_{11}) lower than 233 K. This test is applicable for the regions examined in this study (low altitudes, midlatitudes, and the tropics), but will not necessarily hold true for polar or high-altitude areas. Next, the 0.65-μm channel is used to identify relatively opaque clouds that possess reflectance

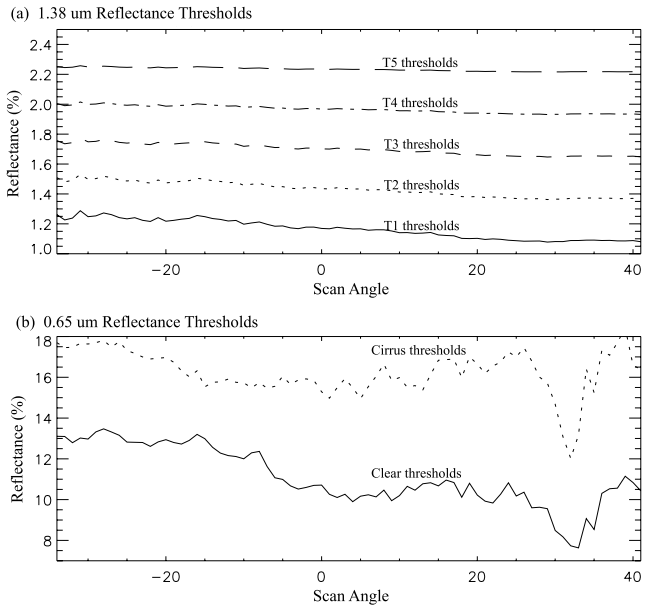

Figure 5. (a) Five 1.38-μm reflectance thresholds and (b) two 0.65-μm reflectance thresholds plotted versus satellite scan angle for an SGP scene (22 March 2001). For this scene, the average solar angle and solar azimuthal angle were 35.9° and 154.6°, respectively. A total of 317,552 pixels was examined. Negative scan angles are defined as those to the right of the satellite path, while positive angles are to the left.

Table 1. Average Threshold Values for the Seven SGP Cases and the Three TWP Cases[a]

Threshold Value	SGP	TWP
$R_{1.38\ T1}$	1.16	1.13
$R_{1.38\ T2}$	1.42	1.41
$R_{1.38\ T3}$	1.69	1.68
$R_{1.38\ T4}$	1.96	1.96
$R_{1.38\ T5}$	2.23	2.23
$R_{0.65\ Tclr}$	11.2	4.2
$R_{0.65\ Tcir}$	17.7	15.6
$BTD_{8.6-11\ Tclr}$	−0.9	−0.57
$BTD_{8.6-11\ Tlow}$	0.76	0.85

[a]SGP stands for southern Great Plains; TWP stands for tropical western Pacific. *R* represents reflectance in percentage. BTD represents brightness temperature difference in kelvins. Clear, cirrus, and low-cloud thresholds are indicated as Tclr, Tcir, and Tlow, respectively.

values greater than both a clear sky and cirrus cloud threshold ($R_{0.65\ Tclr}$ and $R_{0.65\ Tcir}$). Both cirrus tests are then performed. For relatively opaque cloud pixels, cirrus is detected by using the specific 1.38-μm reflectance threshold and/or (depending on which product AND or OR is being produced) the low-cloud $BTD_{8.6-11}$ threshold ($BTD_{8.6-11\ Tlow}$). It is assumed that both opaque single layer cirrus clouds as well as multilayer clouds with a cirrus component are defined in this group. If cirrus is not indicated, then these relatively opaque clouds are thought to be low-level, water clouds. For the nonopaque pixels, thin, single-layer cirrus is identified by the cirrus tests, but using the clear-sky $BTD_{8.6-11}$ threshold instead. If a pixel yet remains unclassified after these tests are performed, it is thought to be clear sky. Nearly 10% of all pixels from the AND product and less than 1% of the pixels from the OR product were classified as clear sky in this manner using the T1 1.38-μm thresholds.

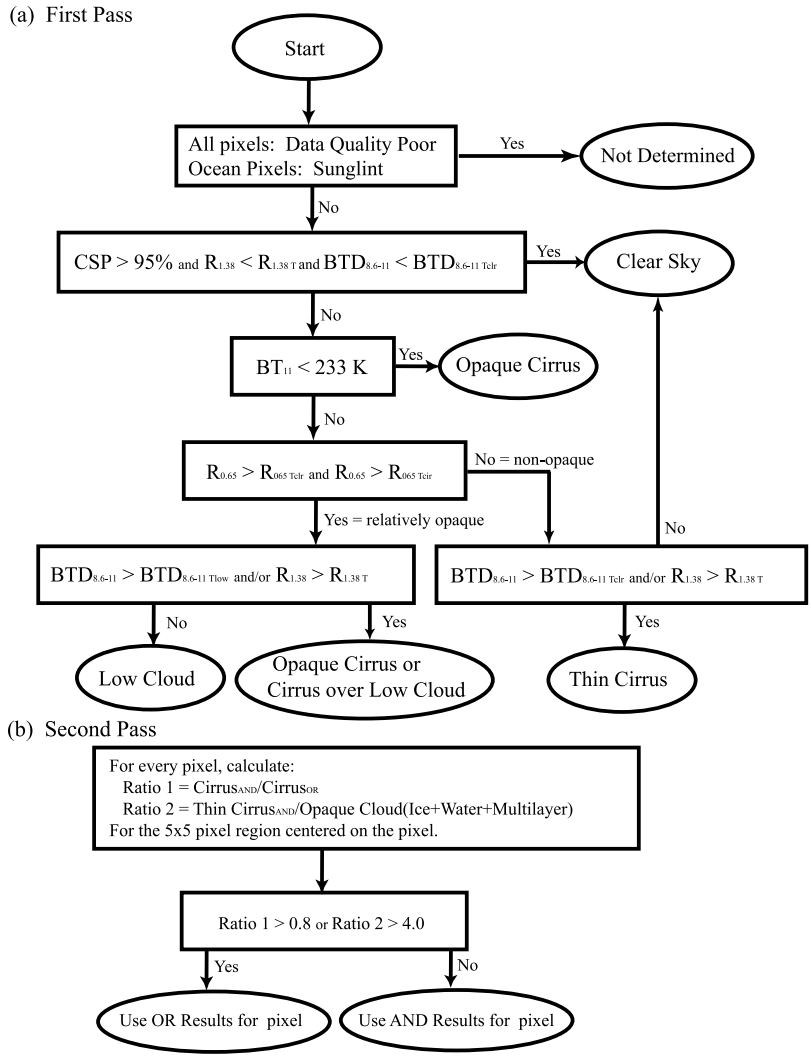

Figure 6. The flowchart describes the new cloud detection scheme. (a) The first pass runs through every pixel and produces two products for every 1.38-μm threshold: the AND product, where positive results from both cirrus tests are used to classify cirrus, and the OR product, where positive results from either cirrus test classify cirrus. (b) The second pass produces a final cloud type product for each 1.38-μm threshold by examining neighboring pixels to decide whether to use the AND or OR results. The letters R, BT, BTD, and T stand for reflectance, brightness temperature, brightness temperature difference, and threshold, respectively. CSP is determined in the MODIS cloud mask product (MOD35).

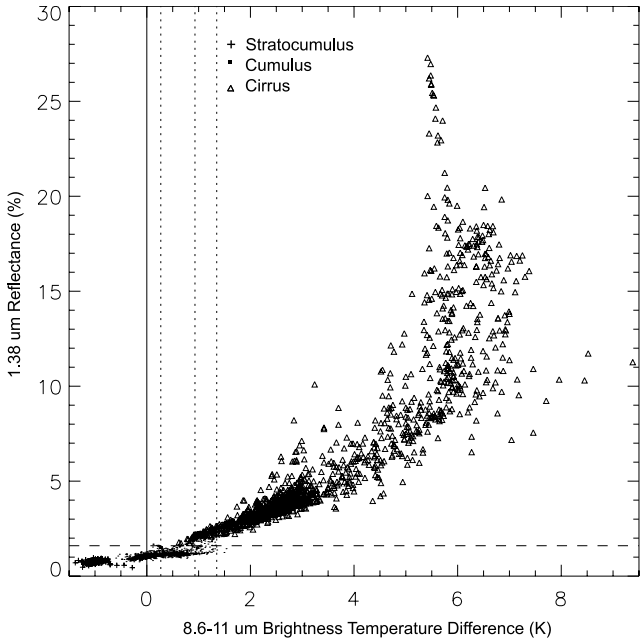

Figure 7. Scatterplot of 1.38-μm reflectance versus 8.6–11 μm BTD for cloudy pixels from three scenes over the ARM-TWP site. Crosses represent stratocumulus clouds on 25 August 2001; dots represent cumulus on 17 August 2001; and triangles show cirrus on 16 August 2001. The dashed horizontal line marks the three scene average T3 1.38-μm reflectance threshold of 1.68%. From left to right, the short dashed vertical lines represent the low-cloud 8.6–11 μm BTD threshold for 25 August, 16 August, and 17 August, respectively.

[16] A final cloud type result for each threshold at a one-pixel resolution is produced in the second pass, Figure 6b, by deciding which result, the AND or the OR, most accurately detects the actual cirrus cloud. The idea is that the OR results can detect more cirrus and will be used unless the risk of falsely identifying low clouds as cirrus is too great due to either a large number of opaque clouds nearby or a major difference between the AND and OR results. Two ratios are calculated using results obtained from the 5 × 5 group of pixels centered on the pixel in question. Ratio 1 is defined as the number of cirrus pixels (single and multilayer) classified by the AND result to the number classified by the OR result. This is a measure of the agreement between the two cirrus tests. If they largely agree (ratio 1 > 0.8), then the OR result is used since there is high confidence that cirrus is present and is being observed. If they do not agree well (ratio 1 < 0.8), the AND result will be used for greater certainty unless it is found, by ratio 2, that there is very little opaque cloud nearby. This ratio is defined as the number of thin cirrus pixels determined from the AND result to the number of opaque cloud pixels. A value of 4.0 is thought to be high enough to show that the region is covered primarily by nonopaque cloud, and also to show that only one cirrus test is sufficient (OR result) and is better able to safely detect cirrus.

[17] In addition to the cloud radar time series, we further compare our cloud type detection results with results from three existing detection schemes. The first is the MODIS cloud phase product, which uses the ratio of $BTD_{8.6-11}$ and BTD_{11-12} described by W. P. Menzel et al. (Cloud top properties and cloud phase algorithm theoretical basis document, ATBD-MOD-04, version 6.0, 62 pp., 2002, available at http://modis.gsfc.nasa.gov/data/atbd/atmos_ atbd.html) and later by *Baum et al.* [2000]. This product is only available at a 5-km resolution. The second is a simple scheme developed by the authors from two MODIS cloud reflectance thresholds tests (0.65 and 1.38 μm) along with the CSP variable and will be named the MODIS cloud mask algorithm. It proves to be a good benchmark since it includes the basic tests in our new scheme yet is not particularly sensitive to thin cirrus because of the relatively high 1.38-μm reflectance threshold used. The last scheme examined was developed by *Ou et al.* [1996] for AVHRR data and will be referred to as the Ou algorithm.

4. Case Studies and Analysis

4.1. TWP Scenes

[18] Figure 7 shows the scatterplot of 1.38-μm reflectances versus $BTD_{8.6-11}$ from cloudy pixels inside a rectangular region defined near the radar for the three TWP cases. The three cases represent three different cloud regimes: stratocumulus, more developed cumulus, and thin cirrus. Points from each scene appear grouped together and are well separated from each other so that the cloud types are easily distinguished as either high or low cloud by the two cirrus tests. Stratocumulus pixels from 25 August 2001, shown by crosses, possess both low 1.38-μm reflectance and $BTD_{8.6-11}$ values. The dots are from cumulus clouds with tops around 2.5 km height on 17 August 2001. These higher clouds have greater $BTD_{8.6-11}$ values but most of the pixels possess 1.38-μm reflectance below the average TWP T3 threshold of 1.68%, shown as the horizontal dashed line. Cirrus pixels (triangles), making up the rest of the points, are from 16 August 2001 and cover a broad range of values lying mainly above both the 1.38-μm reflectance and $BTD_{8.6-11}$ thresholds. The average T3 1.38-μm threshold appears to appropriately separate the high clouds from the lower clouds. The dotted vertical lines represent the low-cloud $BTD_{8.6-11}$ thresholds for 25, 16, and 17 August from left to right. Each adequately partitions low-cloud pixels to its left as smaller values, despite the fact that they vary greatly from scene to scene. As a result, the separation in $BTD_{8.6-11}$ between the higher cumulus pixels of 17 August, and the cirrus pixels of 16 August appears to be less clear as there is a fair amount of overlap in the horizontal ($BTD_{8.6-11}$) direction. The distinction between these cloud clusters is made more clearly by 1.38-μm reflectance.

[19] Table 2 gives the validation results from the comparison of the cirrus detected by each cloud type detection scheme to that observed by the 1-hour millimeter-wave radar time series for cases where cirrus was present. The numbers listed in the table represent, in percentage, the amount of cirrus detected by the cloud type detection schemes that agreed with the cirrus observed by the cloud radar. Values were produced by matching the two-dimensional cloud detection results using the cloud top level wind

Table 2. Results From Comparisons of Cirrus Detected by the Individual Cloud Type Detection Schemes to That of Observed Cirrus by the Millimeter-Wave Radar[a]

Parameter	11 February	6 March	22 March	14 April	16 August
Radar cloud, %	thin ci(100)	thick ci(100)	thin ci(100)	ci(20), st(80)	thin ci(100)
Cloud thickness range, km	0.5–1.5	3.9–5.0	0.7–2.8	ci(0.1–0.5), st(1–2.3)	0.1–2.2
Maximum cloud top, km	10.7	10.5	10.6	ci(8.7), st(2.7)	10.3
Cirrus optical depth range	0.1–0.5	0.8–1.5	0.15–0.9	0.02–0.2	0.02–0.7
Cloud Detection Results	11 February	6 March	22 March	14 April	16 August
NS1[b]	100	100	92	72	100
NS2[c]	100	100	79	59	100
NS3[d]	100	100	74	57	100
NS4[e]	100	100	73	56	100
NS5[f]	100	100	73	54	100
M6[g]	0	100	0	0	41
MCM[h]	1	100	10	52	15
OA[i]	35	100	68	28	94

[a]Only scenes in which cirrus was observed by the radar are included. Numerical values are listed in percentage with the exception of the radar cloud thickness range and radar maximum cloud top height, which are given in kilometers, and the range of cirrus cloud optical depth. Empirical optical depths were calculated using theoretical extinction coefficients produced for ice crystals with effective sizes of 10 and 42 μm [*Liou*, 2002].
[b]New scheme with T1 (lowest) thresholds.
[c]New scheme with T2 thresholds.
[d]New scheme with T3 thresholds.
[e]New scheme with T4 thresholds.
[f]New scheme with T5 thresholds.
[g]MODIS (MOD06) cloud phase product.
[h]MODIS cloud mask algorithm.
[i]*Ou et al.* [1996] algorithm.

to 31 points of the radar time series at 2-min intervals for the period starting 30 min before and ending 30 min after the MODIS overpass. Each radar data point in time was compared to nine cloud type detection pixels from a 3 × 3 square region centered on the single pixel which matched closest to the radar point in time. Therefore 279 points were compared for each case. In addition, Table 2 displays specific fractional cloud type amount, the range in vertical cloud thickness, and the maximum cloud top height observed by the radar as well as approximated cirrus optical depth at 0.5 μm. Optical depth was computed by using radar cloud thickness and theoretical extinction coefficients, calculated for effective ice crystal sizes of 10 and 42 μm described by *Liou* [2002]. The range in optical depth was determined by the maximum and minimum values from calculations involving both size parameters. Only one TWP scene (16 August) is shown as the last case in Table 2.

[20] Statistics from this scene indicate that all of the new cloud type detection scheme results detect cirrus similarly and compare more favorably to the radar ground truth than the other schemes. There was a 100% agreement with the radar in the thin cirrus detected at each 1.38-μm threshold level. This shows that cirrus detection was not dependent upon the threshold level used between T1 and T5. By examining the specific cirrus test results in Table 3, it can also be seen that 100% of the cirrus cloud was detected by both cirrus tests for this scene except when the T5 1.38-μm reflectance threshold was used. Table 3 shows the percentage of cirrus detected by each cirrus test separately as well as by both cirrus tests simultaneously for each of the five 1.38-μm reflectance thresholds. All of the pixels in the

Table 3. High-Cloud Detection Results by Each High-Cloud Test for Every 1.38-μm Reflectance Threshold and the 10 Selected Cases[a]

Threshold	Cirrus Test	11 February	6 March	22 March	29 March	14 April	16 April	25 May	16 August	17 August	25 August
T1	$R_{1.38}$ only	0	0	16.3	65.3	10.4	100	4.9	0	34.8	0
	$BTD_{8.6-11}$ only	0	0	1.5	0	26.9	0	0	0	6.6	7.4
	both	100	100	66.4	0	17.8	0	0	100	27.7	0
T2	$R_{1.38}$ only	0	0	5.5	2	6.9	100	1.7	0	11.2	0
	$BTD_{8.6-11}$ only	0	0	12.4	0	29.8	0	0	0	33.6	7.4
	both	100	100	55.5	0	14.9	0	0	100	0.6	0
T3	$R_{1.38}$ only	0	0	1.6	0	4.4	100	0	0	3.1	0
	$BTD_{8.6-11}$ only	0	0	30.2	0	31.6	0	0	0	33.6	7.4
	both	100	100	37.7	0	13	0	0	100	0.6	0
T4	$R_{1.38}$ only	0	0	0.2	0	1.7	100	0	0	1	0
	$BTD_{8.6-11}$ only	0	0	42.9	0	33.1	0	0	0	33.6	7.4
	both	100	100	25	0	11.5	0	0	100	0.6	0
T5	$R_{1.38}$ only	0	0	0	0	0.5	100	0	0	0	0
	$BTD_{8.6-11}$ only	0	0	49.8	0	34.2	0	0	0.9	34.1	7.4
	both	100	100	18.1	0	10.4	0	0	99.1	0.1	0

[a]Data was examined near the millimeter-wave radar inside a rectangular region defined by the 1-hour cirrus level wind vector centered on the MODIS overpass time. Numerical values are given as percentage of pixels examined. T1 represents the use of the T1 1.38-μm reflectance thresholds in the new cloud type detection scheme. T2 uses the T2 thresholds, and so on. *R* represents reflectance, and BTD represents brightness temperature difference.

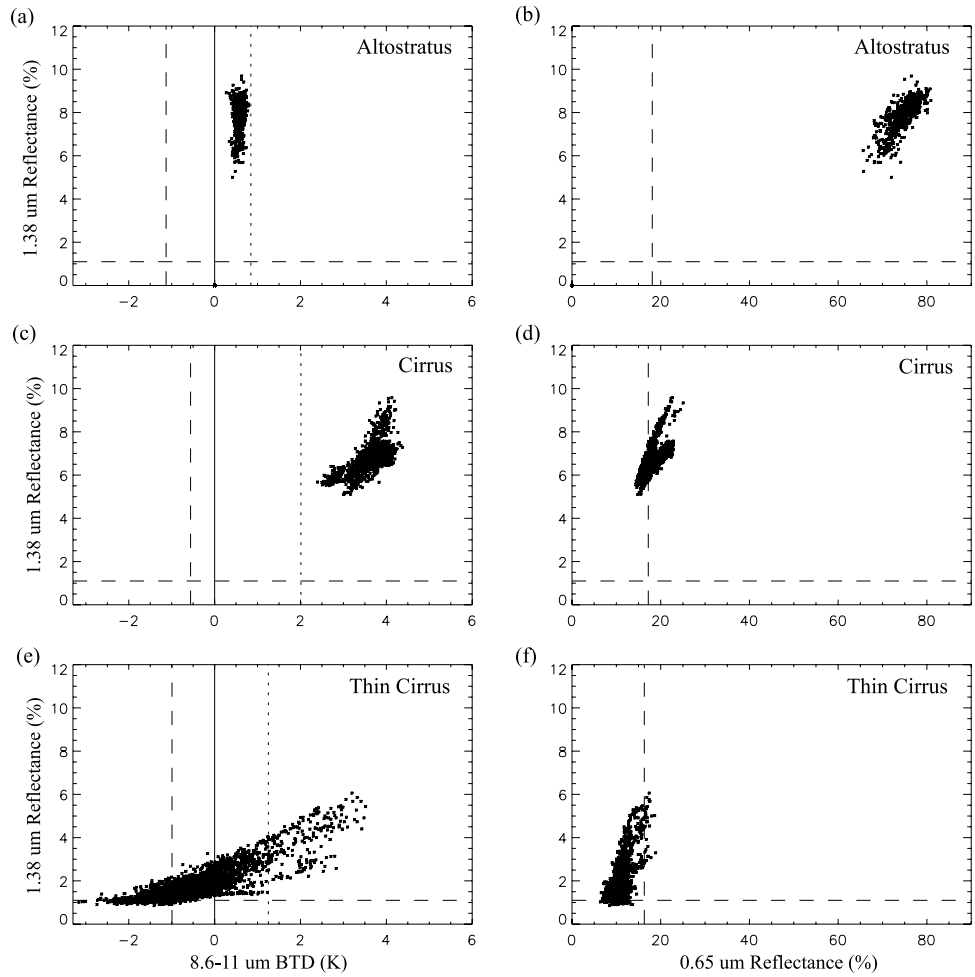

Figure 8. Scatterplots of 1.38-μm reflectance versus 8.6−11 μm BTD for cloudy pixels from three scenes over the ARM-SGP site: (a) midlevel clouds on 16 April 2001, (c) thick cirrus on 6 March 2001, and (e) thin cirrus on 22 March 2001. (b, d, and f) Plotted for the same three scenes is the 1.38- versus 0.65-μm reflectance, respectively. The dashed horizontal lines mark the average T1 1.38-μm reflectance threshold used in each case. The first dashed vertical line in Figures 8a, 8c, and 8e represents the clear 8.6−11 μm BTD threshold, while the short dashed vertical line shows the low-cloud threshold. In Figures 8b, 8d, and 8f the vertical line indicates the average 0.65 μm thin cirrus reflectance threshold. For the 22 March case, 3600 pixels were examined while 1000 pixels were utilized in both the 16 April and 6 March cases.

rectangular region defined by the cloud top wind vector during the 1-hour radar time series used as a diagonal were examined. As such, far more pixels were included in Table 3 than in Table 2.

[21] From Table 3 it is seen that both cirrus tests falsely detected cirrus cloud individually in the cumulus case on 17 August when using the T1 1.38-μm reflectance thresholds. By using a higher 1.38-μm reflectance threshold level, the number of incorrectly detected cirrus pixels decreased dramatically while over 33% of the pixels were still falsely detected by the $BTD_{8.6-11}$ test alone. The previously discussed radiative transfer calculations indicate that optically thin low cloud, perhaps from cloud edges in this case, produce relatively high $BTD_{8.6-11}$ values. By combining the two tests at the higher threshold (>T1), only 0.6% of the pixels were wrongly classified as cirrus. Table 3 also shows that no low cloud was falsely detected as cirrus by any of the new scheme 1.38-μm reflectance threshold levels in the cumulus case on 25 August.

4.2. SGP Scenes

[22] A potential problem in detecting high clouds with the use of the 1.38-μm band is excessive reflection from low levels and the surface. This does not seem to be a problem in the moist tropical troposphere where normally large water vapor concentration lessens low-level reflection, but it may be a concern in the somewhat drier atmospheres over land. Column water vapor measurements from the microwave radiometer were 6, 6, and 4 cm from the three TWP cases of 16 August, 17 August, and 25 August, respectively. On the other hand, column water vapor amounts for the seven SGP scenes were all less than 2 cm except for the 14 April case, which had a value of nearly 3 cm. It is noted that this test is expected to have trouble due to enhanced low-level reflec-

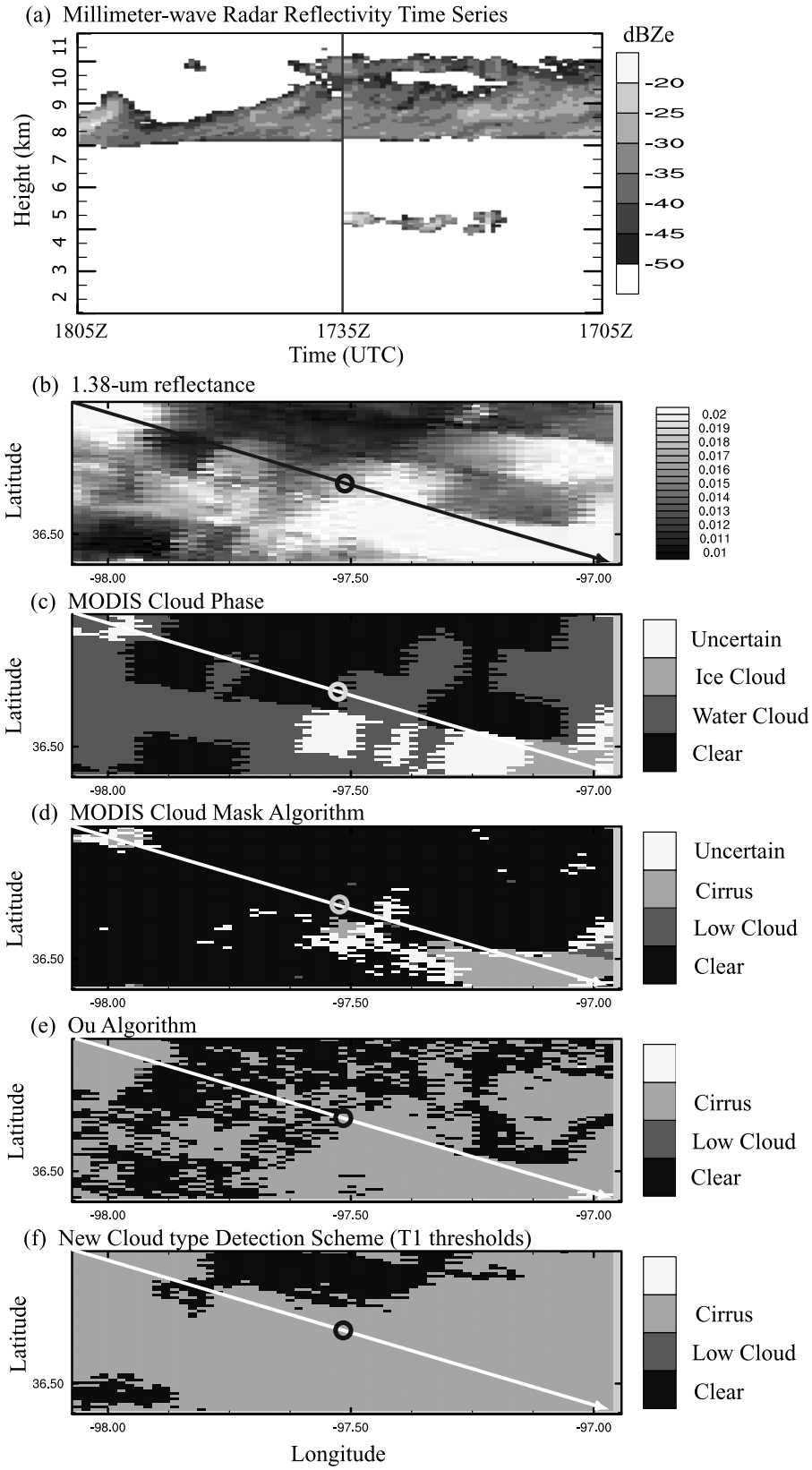
(a) Millimeter-wave Radar Reflectivity Time Series
dBZe
-20
-25
-30
-35
-40
-45
-50
Height (km)
2 3 4 5 6 7 8 9 10 11
1805Z
1735Z
1705Z
Time (UTC)
(b) 1.38-um reflectance
0.02
0.019
0.018
0.017
0.016
0.015
0.014
0.013
0.012
0.011
0.01
Latitude
36.50
-98.00
-97.50
-97.00
(c) MODIS Cloud Phase
Uncertain
Ice Cloud
Water Cloud
Clear
(d) MODIS Cloud Mask Algorithm
Uncertain
Cirrus
Low Cloud
Clear
(e) Ou Algorithm
Cirrus
Low Cloud
Clear
(f) New Cloud type Detection Scheme (T1 thresholds)
Cirrus
Low Cloud
Clear
Longitude

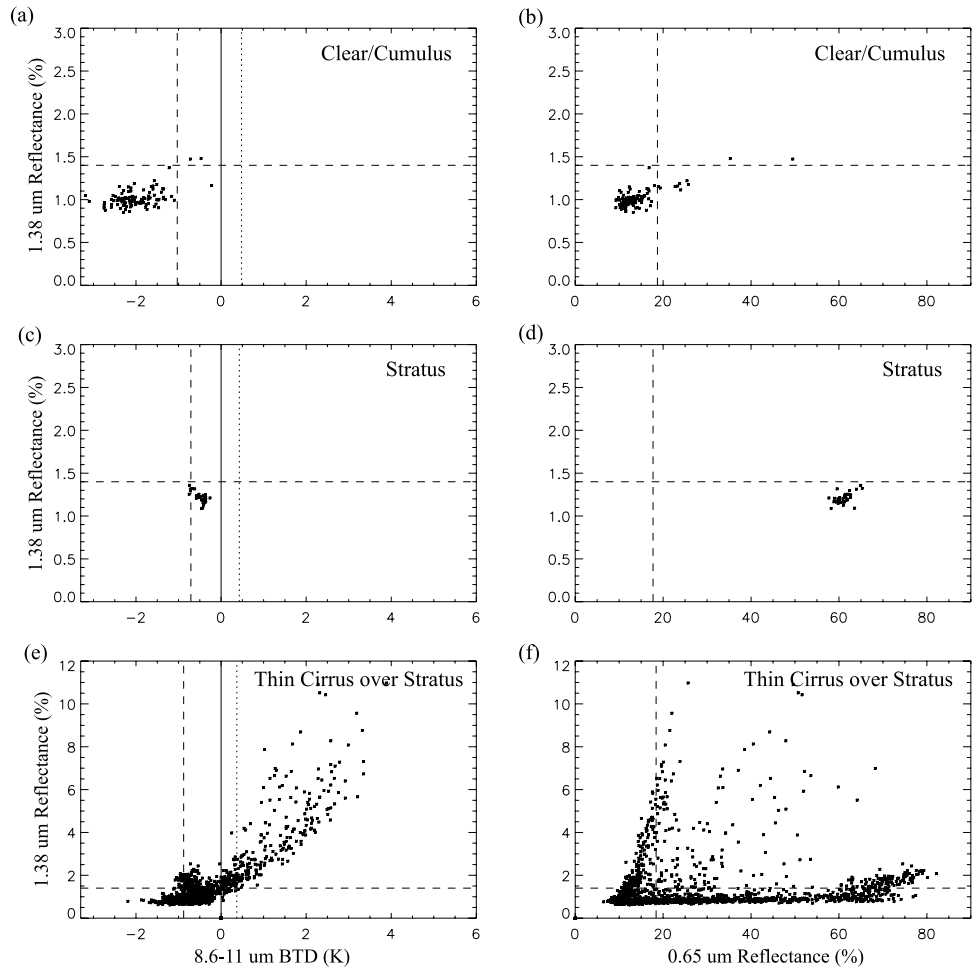

Figure 10. Scatterplots of 1.38-μm reflectance versus 8.6–11 μm BTD for pixels from three scenes over the ARM-SGP site: (a) clear sky and cumulus on 25 May 2001, (c) stratus on 29 March 2001, and (e) thin cirrus over stratus on 14 April 2001. (b, d, and f) Plotted for the same three scenes is the 1.38- versus 0.65-μm reflectance, respectively. The dashed horizontal lines mark the average T2 1.38-μm reflectance threshold used in each case. The first dashed vertical line in Figures 10a, 10c, and 10e represents the clear 8.6–11 μm BTD threshold, while the short dashed vertical line shows the low-cloud threshold. In Figures 10b, 10d, and 10f the vertical line indicates the average 0.65 μm thin cirrus reflectance threshold. For the three cases of 25 May, 29 March, and 14 April, 100, 36, and 1956 pixels were examined, respectively.

tion where the water vapor path is very small such as over deserts and polar regions and at high altitudes.

[23] Figure 8 shows the scatterplot of 1.38-μm reflectance versus $BTD_{8.6-11}$, and separately, versus 0.65-μm reflectance from all pixels in the rectangular region defined by the 1-hour cloud-level wind vector centered at the MODIS overpass time for three different cases over the ARM-SGP site. These three cases represent three different nonlow cloud scenes: midlevel clouds at a height of 4 km from 16 April (Figures 8a and 8b); thick cirrus on 6 March (Figures 8c and 8d); and thin cirrus from 22 March (Figures 8e and 8f). By comparing the midlevel cloud scatterplots to those of the cirrus, one can see how relatively opaque cirrus is differentiated from high-altitude (4 km) opaque water clouds using only the 0.65-μm reflectance and the $BTD_{8.6-11}$. In both cases, the 1.38-μm reflectance is large (vertical axes) and much greater than any of the five thin cirrus thresholds of which only one, T1 (horizontal dashed line), is drawn. For the midlevel cloud case, this is most likely due to the low column water vapor amount of 1.7 cm which was measured.

Figure 9. (opposite) (a) The 1-hour time series of the millimeter-wave radar reflectivity based at the central facilities of the ARM-SGP site in Lamont, Oklahoma, centered on the MODIS overpass on 22 March 2001 at 1735 UT (vertical line). For the same scene, (b) 1.38-μm reflectance and (c) MODIS cloud phase. Cloud detection results from the (d) MODIS cloud mask algorithm, (e) Ou algorithm, and (f) new scheme using the T1 thresholds. Areas of white appearing in Figures 9c and 9d represent uncertain cloud type. The vectors represent the 8-km wind during the 1-hour period surrounding the MODIS overpass. The circles mark the location of the millimeter-wave radar.

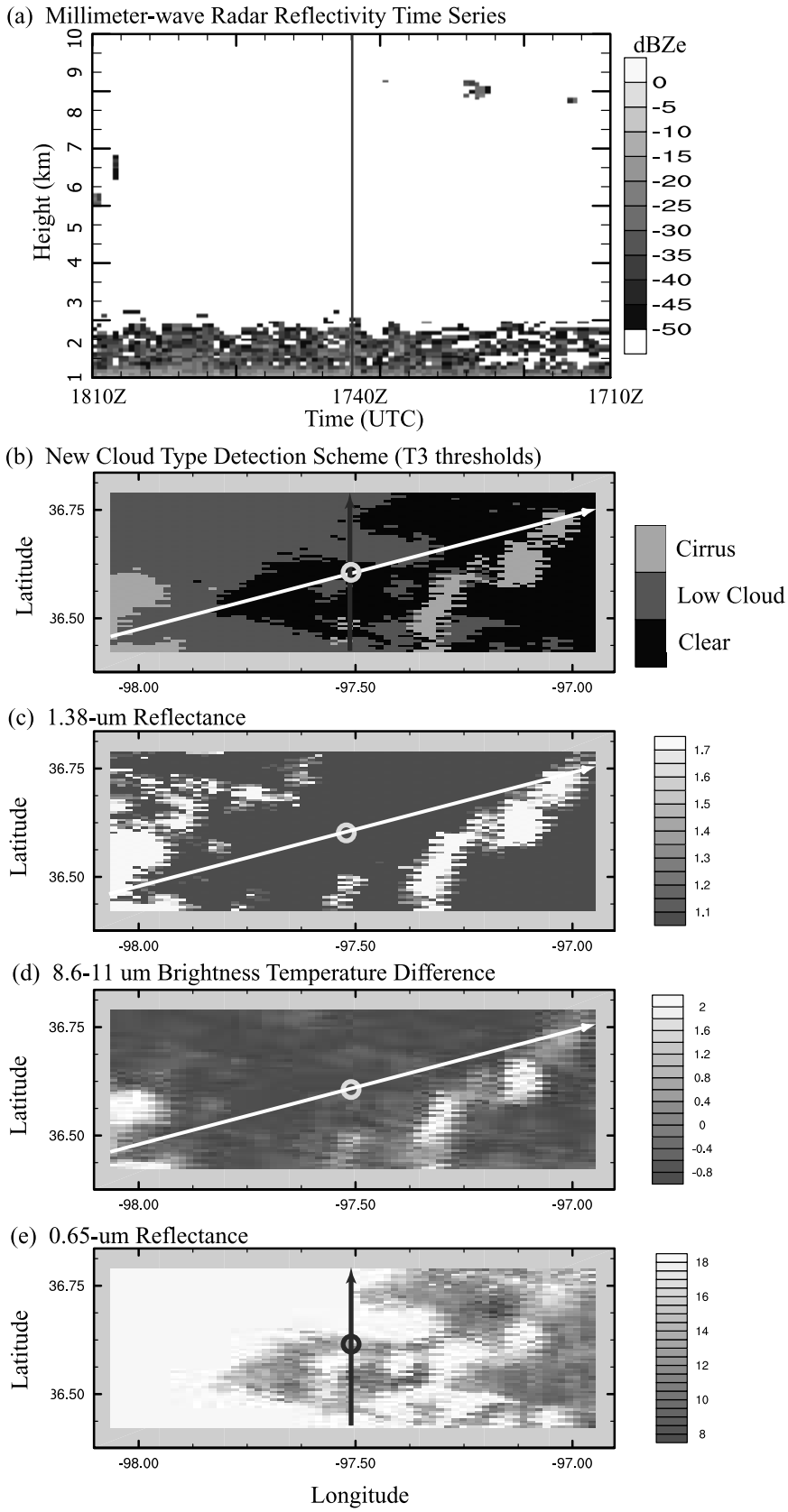
(a) Millimeter-wave Radar Reflectivity Time Series
dBZe
0
-5
-10
-15
-20
-25
-30
-35
-40
-45
-50
Height (km)
1
2
3
4
5
6
7
8
9
10
1810Z
1740Z
1710Z
Time (UTC)
(b) New Cloud Type Detection Scheme (T3 thresholds)
Latitude
36.75
36.50
-98.00
-97.50
-97.00
Cirrus
Low Cloud
Clear
(c) 1.38-um Reflectance
Latitude
36.75
36.50
-98.00
-97.50
-97.00
1.7
1.6
1.5
1.4
1.3
1.2
1.1
(d) 8.6-11 um Brightness Temperature Difference
Latitude
36.75
36.50
-98.00
-97.50
-97.00
2
1.6
1.2
0.8
0.4
0
-0.4
-0.8
(e) 0.65-um Reflectance
Latitude
36.75
36.50
-98.00
-97.50
-97.00
18
16
14
12
10
8
Longitude

Since all of the midlevel cloud pixels also possess high 0.65-μm reflectance, the low-cloud $BTD_{8.6-11}$ threshold (short dashed vertical line) is employed, and because the $BTD_{8.6-11}$ values are less than this threshold, we classify these clouds as being of water phase. Radiosonde data support this water phase characterization since cloud temperature was measured to be between 2° and −5°C. Regardless of whether the 0.65-μm reflectance identifies some of the cirrus pixels from 6 March as relatively opaque or not, all of the pixels are detected as cirrus by both the clear-sky (long dashed vertical line) and low-cloud $BTD_{8.6-11}$ thresholds. The cirrus from 6 March was correctly detected by both cirrus tests (Table 3) and easily identifiable by every cloud type detection scheme with 100% accuracy when compared to the cloud radar as shown in Table 2. Every cloud type detection scheme except the MODIS cloud mask was also able to correctly classify the altostratus clouds of 16 April as noncirrus (not shown). The MODIS cloud mask scheme had trouble because the large 1.38-μm reflectance produced by these midlevel clouds characterized them as high clouds. Results from Table 3 show that all of the 1.38-μm reflectance thresholds in the new cloud type detection schemes also identified the altostratus as cirrus but, because the additional $BTD_{8.6-11}$ test did not detect these clouds as cirrus, the final new scheme results were 100% correct.

[24] The thin cirrus case of 22 March presents a different scenario. The low 0.65-μm reflectance indicates that nearly all of the clouds were nonopaque so that their $BTD_{8.6-11}$ values were compared to the clear-sky threshold instead. Although most of the pixels were classified as cirrus because the $BTD_{8.6-11}$ values were larger than the clear-sky threshold, some pixels still remained undetected by this test. On the other hand, it can be seen that the majority of the pixels with $BTD_{8.6-11}$ values less than the clear-sky threshold have 1.38-μm reflectance greater than the average T1 1.38-μm reflectance threshold and therefore are detectable by the 1.38-μm reflectance threshold test. By examining the results in Table 2, it is seen that all of the new cloud type detection algorithms detected far more thin cirrus observed by the radar than the other cloud type detection schemes. Figure 9 displays the two-dimensional horizontal plots of 1.38-μm reflectance, the MODIS cloud phase, MODIS cloud mask algorithm, Ou algorithm, and new cloud type detection results using the T1 1.38-μm reflectance thresholds along with the 1-hour millimeter-wave radar time series. The rectangular regions shown were determined by using the 1-hour cirrus level wind vector as a diagonal and the data contained inside were used to generate the scatterplots in Figures 8e and 8f. The radar time series is given in reverse time units (horizontal axis) so that clouds observed later by the radar can match those clouds along the wind vector in the spatial cloud type detection plots which were located west of the radar (circles) at the time of the MODIS overpass (1735 UT), and clouds seen earlier can match those detected east of the radar. It can be seen that the 1.38-μm reflectance along the wind vector is somewhat proportional to the actual cirrus thickness. For example, the lowest reflectance occurs when the cloud is at its thinnest. The new cloud type detection scheme cirrus coverage mimics the 1.38-μm reflectance pattern to a large extent and is clearly in best agreement with the radar along the wind vector. The Ou algorithm also performs well but is unable to detect the thinnest cirrus.

[25] It is also apparent from Table 2 that the thin cirrus detection of 22 March is improved by lowering the 1.38-μm thresholds and that the T1 thresholds recorded the highest agreement (92%) with the radar. In fact, changing from the T2 to the T1 thresholds represented the largest improvement. Results from Table 3 indicate that by using the threshold levels from T2 to T5, the $BTD_{8.6-11}$ test detected more thin cirrus than the 1.38-μm reflectance test. Only by using the T1 thresholds did the 1.38-μm test out perform the $BTD_{8.6-11}$ test, and as a result, obtain cloud type results closer to the cloud radar observations.

[26] The new cloud type detection algorithm also detected more thin cirrus in the other single-layer thin cirrus case over the SGP site (11 February). Table 2 shows that there was 100% agreement with the cloud radar for every 1.38-μm reflectance threshold level while the second best results from the Ou scheme only produced 35% agreement. Since there was no distinction between the differing 1.38-μm reflectance thresholds in this case, cirrus reflection must have been greater off the 11 February clouds than off those on 22 March. Even though results from Table 3 show that both high-cloud tests correctly identified thin cirrus equally perfect, the $BTD_{8.6-11}$ thresholds appear to be affected by substantial variance from scene to scene more so than the 1.38-μm reflectance thresholds. As a result, it is suggested that the 1.38-μm reflectance test is more sensitive to thin cirrus for scenes involving transparent clouds, but the $BTD_{8.6-11}$ test more accurately detects cirrus when opaque water clouds exist, as seen from the scatterplot in Figure 8a. It seems clear, as a result of the specific values from Figure 8, that the likelihood of our new cloud type detection algorithm detecting very thin clouds situated above opaque midlevel clouds is poor because $BTD_{8.6-11}$ values of thin cirrus and those of altostratus are similar, while 1.38-μm reflectance off midlevel clouds is actually greater than that off thin cirrus. Fortunately, the simultaneous occurrence of cirrus and midlevel cloud is infrequent. *Tian and Curry* [1989] observed cirrus over midlevel cloud only 11% of the time by analyzing vertical distributions of clouds using the Air Force three-dimensional nephanalysis procedure over the North Atlantic Ocean. This number included all types of cirrus, so the thin cirrus percentage is expected to be lower.

[27] Figure 10 shows the $BTD_{8.6-11}$ and 0.65-μm reflectance versus 1.38-μm reflectance scatterplots for the three

Figure 11. (opposite) (a) The 1-hour time series of the millimeter-wave radar reflectivity based at the central facilities of the ARM-SGP site in Lamont, Oklahoma, centered on the MODIS overpass on 14 April 2001 at 1745 UT (vertical line). For the same scene, the new cloud type detection scheme results using the (b) T3 1.38-μm reflection thresholds, (c) 1.38-μm reflectance, (d) 8.6–11-μm BTD, and (e) 0.65-μm reflectance. The light vectors indicate the direction and speed of the 8-km wind during the 1-hour period surrounding the MODIS overpass, while the dark vectors represent the 1-km wind. The circles mark the location of the millimeter-wave radar.

cases involving low clouds. Both the cumulus pixels of 25 May (Figures 10a and 10b) and the stratus pixels of 29 March (Figures 10c and 10d) are clearly identified as low cloud or clear sky by possessing low 1.38-μm reflectance and low $BTD_{8.6-11}$ values. Table 3 shows that 4.9% of the pixels in a rectangular region surrounding the radar were incorrectly classified as cirrus by the T1 thresholds in the 25 May case. The T1 thresholds also mistakenly detected 65% of the stratus pixels of 29 March as cirrus. Both of these percentages dramatically decreased when the T2 thresholds were employed and disappeared completely by using the T3 thresholds. These cases suggest that when opaque cloud is detected, the T3 cirrus 1.38-μm reflectance thresholds should be employed.

[28] The scatterplot for the 14 April case (Figures 10e and 10f) in which thin cirrus was observed over stratus is dramatically different than the other two low-cloud cases. The scatter in the plot results from the four cloudiness regimes: clear-sky, low-cloud, single-layer cirrus, and multilayer cloud in which thin cirrus overrides stratus. The bulk of the pixels possesses both low 1.38-μm reflectance and $BTD_{8.6-11}$ values but is spread across a large range of 0.65-μm reflectance values. These qualities are generally attributable to a low-cloud field of variable optical depth and intermittent clear patches. The gradual increase in both 1.38-μm reflectance and $BTD_{8.6-11}$ in Figure 10e is characteristic of cirrus. Many of these points correspond to the steep rise in 1.38-μm reflectance near the average thin cirrus 0.65-μm reflectance threshold (long dashed vertical line) in Figure 10f, which is common for single-layer cirrus pixels. The remaining points with larger 0.65- and 1.38-μm reflectance are most likely due to multilayer cloud since it is known that thick high cloud did not exist near the radar.

[29] The millimeter-wave radar observed thin cirrus with maximum thickness of 500 m at 8–9 km height then later at 5.5–7 km about 20% of the time. More frequently observed, about 80% of the time, was low cloud with a maximum cloud top height of 2.7 km. Using the radar information as ground truth, Table 2 shows that the new cloud type detection scheme detected more of the cirrus observed by the radar than the other cloud type detection schemes. The T1 1.38-μm reflectance threshold version achieved the greatest agreement (72%). Not shown in the table is the percentage of cirrus detected by the cloud type detection schemes where no cirrus was observed by the radar. These values were 21, 18, 16, 12, and 9% for the new scheme results using the T1, T2, T3, T4, and T5 1.38-μm reflectance thresholds, respectively. Also, values of 0 and 29% were recorded by the MODIS cloud mask scheme and the Ou algorithm, respectively. This extra cirrus detected may be partially due to the difficulty in matching spatial points to the time series. Table 3 shows that despite the large amount of cirrus identified individually by the two cirrus tests, they simultaneously detected cirrus between 10.4 and 17.8% of the time. The highest value of 17.8%, from the T1 thresholds, correlates well with the 20% total cirrus coverage observed by the radar. Since the MODIS cloud mask 1.38-μm reflectance threshold test, used for high-cloud detection in our MODIS cloud mask scheme, identified only 52% of the radar observed cirrus, it appears that the MODIS operational 1.38-μm reflectance thresholds in the cloud mask product may not have been sensitive to very thin cirrus.

[30] Figure 11a plots radar reflectivity in reverse time sequence in order to match points along the cirrus level wind vector (white arrow) in the two-dimensional spatial plots in Figures 11b–11d. The dark vector represents the 1-km level wind in plots of Figures 11b and 11e. The location of the tips of both vectors match to the earliest time of 1710 UT in the radar time series and the vector tails match the latest time, 1810 UT. Both vectors define the area of the rectangular regions shown and thus the data that were utilized to generate the scatterplots in Figures 10e and 10f. It can be seen that the new cloud type detection scheme with the T3 1.38-μm reflectance thresholds shown in Figure 11b detected too much clear sky near the radar, which is seen as low cloud in the radar time series. Table 3 results show that the $BTD_{8.6-11}$ test detected much more false high cloud than did the 1.38-μm reflectance test in this case. This may be in part due to the rather large column water vapor amount (3 cm) measured in the scene, which was nearly twice that of all other SGP cases. This can also be seen by examining the two-dimensional plots in Figure 11c of 1.38-μm reflectance, Figure 11d of $BTD_{8.6-11}$, and Figure 11e of 0.65-μm reflectance. Each is plotted using scales that highlight specific thresholds. For example, the minimum value of 1.1% in Figure 11c represents the average T1 1.38-μm reflectance threshold. Since most of the area near the radar appears dark in this figure, indicating that 1.38-μm reflectance was less than the minimum plot value of 1.1% corresponding to the average T1 1.38-μm reflectance threshold, the 1.38-μm reflectance test is not responsible for the false detection of cirrus in this region. The $BTD_{8.6-11}$ plot, however, shows values slightly above the clear-sky threshold of −0.8 K used as the minimum scale throughout the region. This threshold is used to classify pixels as cirrus when nonopaque cloud exists. Plot in Figure 11e shows that all of the nonwhite shaded area near the radar represents nonopaque cloud since the average cirrus 0.65-μm reflectance threshold for this scene was near 18% which was used as an upper bound in the scaling. As a result, these pixels with low $BTD_{8.6-11}$ occurring in region of nonopaque cloud as determined by 0.65-μm reflectance are classified as cirrus even though their low $BTD_{8.6-11}$ values were marginally higher than the clear-sky threshold and their 1.38-μm reflectance was well below even the lowest cirrus threshold. Probably, these false cirrus pixels were actually semitransparent low clouds, which are expected to possess slightly higher $BTD_{8.6-11}$ values than clear sky. These clouds can also produce high 11–12 μm BTD values which are used to detect high clouds in the Ou algorithm and may be responsible for the large number of additional cirrus detected by that scheme. Forcing the AND version of the cirrus tests to be used when results from the two cirrus tests do not agree regardless of the high amount of nonopaque cloud present, eliminated this false cirrus detection in this case, but instead, produced clear-sky pixels as seen in Figure 11b. Much of the semitransparent low cloud in this scene remained undetected by the new cloud type detection algorithm since only opaque low cloud can be detected with high 0.65-μm reflectance.

[31] The cirrus shown later in the radar time series, located in the western part of the region along the upper level wind vector in the spatial plots of Figure 11, was identified well by the new cloud type detection scheme, but

much of the earlier cirrus in the time series was not detected. A substantial amount of cirrus seen in Figure 11b lies just south of the upper level wind vector in the eastern section of the plot but may have been that observed by the radar. Inaccuracies in the measured wind direction can produce large errors when matching the spatial locations to the time series. By giving the upper level wind vector a more westerly alignment, the new cloud type detection scheme results would agree more with the radar. In any case, the results from this case indicate that thin cirrus can be identified by our new cloud type detection algorithm even when substantial low cloud is present when the column water vapor path is relatively large near 3 cm.

5. Conclusions

[32] A new daytime cloud detection scheme was developed to take advantage of the cirrus cloud detection capabilities of the MODIS 1.38-μm band. Reflectance in the 1.38-μm channel varies significantly and is dependent on viewing geometry, cloud properties and height, and the vertical atmospheric water vapor concentration. Our new cloud detection scheme tries to adjust to the specific state of the atmosphere by determining 1.38-μm reflectance thresholds based on mean clear-sky reflectance on a scene-by-scene basis. To account for different viewing angles, 1.38-μm thresholds were determined only as a function of sensor scan angle since the solar angles for each MODIS granule do not vary significantly. $BTD_{8.6-11}$ also exhibits excellent skill in detecting thin cirrus and is used together with the 1.38-μm reflectance test to form a more sophisticated thin cirrus identification procedure.

[33] Through the examination of 10 MODIS cloud scenes of varying structures, we have established two sets of cirrus test thresholds determined by visible reflectance. In regions of low visible reflectance, 1.38-μm reflectance and $BTD_{8.6-11}$ thresholds should be calculated from clear-sky pixels with levels slightly above mean values. Where visible reflectance is high, $BTD_{8.6-11}$ thresholds should be calculated from low-cloud pixels and 1.38-μm reflectance thresholds are best set roughly three times further from the mean values than they were in the low visible reflectance regions to account for the slightly enhanced low-level reflectance.

[34] We performed validation by collocating two-dimensional cloud detection results at one moment in time with a single vertical cloud radar profile over a period in time. Only those pixels aligned with the cloud level wind passing over the radar during a 1-hour period surrounding a MODIS overpass were strictly examined. The thin cirrus detected from our new scheme correlated well with data from the cloud radar time series. In all of the cases, statistics provided evidence that our new scheme detected more cirrus seen by the radar than existing cloud type detection schemes. The major results drawn from this study are as follows. First, detection of single-layer thin cirrus was dramatically increased. Second, a greater amount of thin cirrus was detected over low cloud by the new scheme in one case. This was the only case as such studied and it possessed a high column water vapor total compared to that of the other land scenes. Third, although our new algorithm was able to decipher thin cirrus and opaque midlevel cloud separately, it is likely that it would not be able to do so if the thin cirrus lied directly above the midlevel cloud due to the similar values of both 1.38-μm reflectance and $BTD_{8.6-11}$ produced by each cloud type. Fortunately, this type of cloud arrangement appears to exist infrequently as pointed out previously in the text. Finally, nonopaque low clouds can be falsely identified as cirrus by the $BTD_{8.6-11}$ test using the nonopaque thresholds. To avoid this mistake, strict agreement with the cirrus 1.38-μm reflectance test is necessary but may result in optically thin low clouds being classified as clear sky.

[35] The new cloud detection scheme appears to be able to dramatically improve the detection of thin cirrus occurring in a single layer as well as when cirrus lies over low cloud, especially when column water vapor amounts are large. Used in regions similar to that of the two ARM sites where data were studied in this paper, this method may do well to complement existing cloud type detection procedures. Examination of more scenes involving thin cirrus over low cloud is needed to establish a minimum cirrus cloud optical depth that can be detected in the presence of lower clouds. More extensive study over the tropical oceans and moist low-elevation continental landmasses as well as other regions such as subpolar oceans and drier landmasses is needed. Further examination into specific 1.38-μm reflectance thresholds based on latitude and season as well as its dependence to the above cloud water vapor path would be useful.

[36] **Acknowledgments.** We obtained MODIS data from the NASA GES DAAC center and millimeter-wave radar reflectivity data from the University of Utah website (http://www.met.utah.edu/mace/homepages/research/eos.html). Data were obtained from the ARM Program sponsored by the U.S. Department of Energy, Office of Science, Office of Biological and Environmental Research, Environmental Sciences Division. This research was supported by AFOSR grant F49620-01-1-0057, DOE grant DE-FG03-00ER62904, and NASA grants NAG5-7123 and NAG5-7738. We would like to thank Steve Ou for his invaluable advice and insight in this topic as well as Chris Moeller of the University of Wisconsin for his procedure that removed the 1.24-μm contamination from the 1.38-μm MODIS data.

References

Baum, B. A., P. F. Soulen, K. I. Strabala, M. D. King, S. A. Ackerman, W. P. Menzel, and P. Yang, Remote sensing of cloud properties using MODIS airborne simulator imagery during SUCCESS: 2. Cloud thermodynamic phase, *J. Geophys. Res.*, *105*, 11,781–11,792, 2000.

Downing, H. D., and D. Williams, Optical constants of water in the infrared, *J. Geophys. Res.*, *80*, 1656–1661, 1975.

Gao, B.-C., A. F. H. Goetz, and W. J. Wiscombe, Cirrus cloud detection from airborne imaging spectrometer data using the 1.38-μm water vapor band, *Geophys. Res. Lett.*, *20*, 301–304, 1993.

Heymsfield, A. J., and C. M. R. Platt, A parameterization of the particle size spectrum of ice clouds in terms of the ambient temperature and the ice water content, *J. Atmos. Sci.*, *41*, 846–855, 1984.

Hutchinson, K. D., and N. J. Choe, Application of 1.38 μm imagery for thin cirrus detection in daytime imagery collected over land surfaces, *Int. J. Remote Sens.*, *17*(17), 3325–3342, 1996.

King, M. D., et al., Airborne scanning spectrometer for remote sensing of cloud, aerosol, water vapor and surface properties, *J. Atmos. Oceanic Technol.*, *13*, 777–793, 1996.

Liou, K. N., *An Introduction to Atmospheric Radiation*, 583 pp., Academic, San Diego, Calif., 2002.

Ou, S. C., K. N. Liou, and B. A. Baum, Detection of multilayer cirrus cloud systems using AVHRR data: Verification based on FIRE-II IFO composite measurements, *J. Appl. Meteorol.*, *35*, 178–191, 1996.

Ou, S. C., K. N. Liou, M. D. King, and S. C. Tsay, Remote sensing of cirrus cloud parameters based on a 0.63–3.7 μm radiance correlation technique applied to AVHRR data, *Geophys. Res. Lett.*, *26*, 2439–2440, 1999.

Rolland, P., and K. N. Liou, Surface variability effects on the remote sensing of thin cirrus optical and microphysical properties, *J. Geophys. Res.*, *106*, 22,965–22,977, 2001.

Rolland, P., K. N. Liou, M. D. King, S. C. Tsay, and G. M. McFarquhar, Remote sensing of optical and microphysical properties of cirrus clouds using moderate-resolution imaging spectroradiometer channels: Methodology and sensitivity to physical assumptions, *J. Geophys. Res.*, *105*, 11,721–11,738, 2000.

Takano, Y., and K. N. Liou, Solar radiative transfer in cirrus clouds, part I, Single-scattering and optical properties of hexagonal ice crystals, *J. Atmos. Sci.*, *46*, 3–19, 1989a.

Takano, Y., and K. N. Liou, Solar radiative transfer in cirrus clouds, part II, Theory and computation of multiple scattering in an anisotropic medium, *J. Atmos. Sci.*, *46*, 20–36, 1989b.

Tian, L., and J. A. Curry, Cloud overlap statistics, *J. Geophys. Res.*, *94*, 9925–9935, 1989.

Warren, S. G., Optical constants of ice from the ultraviolet to the microwave, *Appl. Opt.*, *23*, 1206–1225, 1984.

Wylie, D. P., W. P. Menzel, H. M. Woolf, and K. I. Strabala, Four years of global cirrus cloud statistics using HIRS, *J. Clim.*, *7*, 1972–1986, 1994.

K. N. Liou and J. K. Roskovensky, Department of Atmospheric Sciences, University of California, 405 Hilgard Avenue, Los Angeles, CA 90095, USA. (jrosko@atmos.ucla.edu)